Signal Processing 134 (2017) 139–148

Contents lists available at ScienceDirect

Signal Processing

journal homepage: www.elsevier.com/locate/sigpro

A multichannel compressed sampling method for fractional bandlimited signals

Haoran Zhao[a], Jingchao Zhang[a], Liyan Qiao[a,*], YangQuan Chen[b]

[a] Department of Automatic Test and Control, Harbin Institute of Technology, Harbin 150086, China
[b] Mechatronics, Embedded Systems and Automation (MESA) Lab, University of California, Merced, USA

ARTICLE INFO

Keywords:
Fractional Fourier Transform
Fractional multiband signals
Modulated wideband converter
Compressed sensing

ABSTRACT

This paper presents a multichannel compressed sampling scheme based on the *modulated wideband converter* and the fractional Fourier transform. The system consists of modulators, analog filters, and analog-to-digital converters. The analog signal is multiplied by a chirp signal and a bank of periodic waveforms. After filtering, the product is uniformly sampled at a rate that is considerably lower than the Nyquist rate. The proposed method which is valid for fractional multiband signals is proven based on the fractional Fourier series. The robustness, recovery accuracy and influence of the fractional order are analyzed by the empirical probability of the successful recovery and the mean squared error.

1. Introduction

Fractional order theory has been developed for many years. The research on fractional order theory has experienced its boom. The fractional Fourier transformation (FrFT) was developed by Namias as a generalization of the standard Fourier transform (FT) and a tool in quantum mechanics [1]. FrFT was a new tool for signal processing until the fast digital computational algorithms were introduced [2–5]. Recently, FrFT has received considerable attention due to its numerous applications, such as signal reconstruction, image processing, neural networks, pattern recognition, radar, sonar, communication, information security and so forth [6–10].

Due to the advantages of FrFT in signal processing, many traditional signal processing theories in the frequency domain (FD) have been extended to the fractional Fourier domain (FrFD) based on the relationship between FrFT and FT, such as the Shannon-Nyquist sampling law [11]. The multichannel sampling structures of fractional bandlimited signals have been studied [9,12,13]. Xu and Tao [14] introduced a randomized nonuniform sampling and reconstruction method. Liu and Bhandari [15,16] employed FrFT to achieve a shift-invariant function by forming an orthogonal basis and a Riesz basis. However, implementations of these existing extensions may be inefficient due to the high sampling rate. To reduce the computational load and save the storage space, compressed samplings are typically required in a fractional signal processing system.

In most scenarios, the carrier frequency of the signal is unknown. Designing a receiver at a sub-Nyquist rate is a challenging task. Compressed sensing (CS) is introduced to collect the information directly, which creatively performs the sampling and compressing at the same time [17–19]. It breaks through the limitations of the conventional Nyquist theorem and greatly reduces the sampling pressure, signal processing rate and the storage capacity [20]. Recently, Mishali and Eldar [21] proposed a novel compressed sampling architecture for multiband signals called the *modulated wideband converter* (MWC). Along with the development of the MWC system, the hardware prototype of the MWC system has been shown [22,23]. A generalized MWC in the FrFD was proposed in [24]. The extended system can recover the fractional bandlimited signal with a normal filter and low sampling rate, but the recovery probability would be very low since the constructed sparse representation is not shift invariant. Most research efforts have focused on the compressed sampling theorem expansions for the bandlimited signal in FD from different perspectives [25,26], but few have focused on the fractional bandlimited signals. It is necessary to generalize a compressed sampling theorem for bandlimited signals in the FrFD.

Our main contribution is a compressed sampling method in the FrFD that constructs a sparse representation for fractional bandlimited signals. We describe how to construct a sub-Nyquist system using modulators, low-pass filters and ADCs; how to choose the parameters of the compressed sampling such that an unique multiband signal can be completely recovered; and how to recover the signal by the framework of compressed sensing. The reminder of this paper is organized as follows. In Section 2, the problem formulation is introduced based on the basic preliminaries. In Section 3, a compressed sampling method

* Correspondence to: Room 526, Bld 2A, Science Park of Harbin Institute of Technology. No.2, Yikuang Street, Harbin, China.
E-mail address: qiaoliyan@163.com (L. Qiao).

http://dx.doi.org/10.1016/j.sigpro.2016.11.023
Received 27 July 2016; Received in revised form 2 November 2016; Accepted 29 November 2016
Available online 08 December 2016

for fractional multiband signals is proposed. The parameters are appropriately selected based on the analysis in the FrFD. In Section 4, the performance of the proposed sampling scheme is analyzed in terms of the robustness, recovery accuracy and influence of the fractional order.

2. Preliminaries

2.1. Fractional Fourier Transform

The fractional Fourier transform (FrFT) is a generalized version of the traditional continuous Fourier transform, which essentially allows the signal in the time-frequency domain to be projected onto a line of arbitrary angle [2]. The definition is denoted by:

$$F_\alpha(u)=\mathcal{F}^\alpha\{f(t)\}=\int_{-\infty}^{+\infty}K_\alpha(u,t)f(t)\mathrm{d}t, \tag{1}$$

where $\mathcal{F}^\alpha$ denotes the FrFT operator. The kernel function $K_\alpha(u,t)$ is as follows:

$$K_\alpha(u,t)=\begin{cases}A_\alpha e^{j\frac{t^2+u^2}{2}\cot\alpha-jtu\csc\alpha}, & \alpha\neq k\pi\\ \delta(u-t), & \alpha=2k\pi\\ \delta(u+t), & \alpha=(2k+1)\pi\end{cases}, \tag{2}$$

where $A_\alpha=\sqrt{\frac{1-j\cot\alpha}{2\pi}}$. $\csc\alpha=\frac{1}{\sin\alpha}$. $k\in\mathbb{Z}$.

The inverse FrFT operator is $\mathcal{F}^{-\alpha}$ which is denoted as follows:

$$K_{-\alpha}(u,t)=A_{-\alpha}e^{-j\frac{u^2+t^2}{2}\cot\alpha+jut\csc\alpha}. \tag{3}$$

In contrast to the standard Fourier analysis, FrFT is suitable for the analysis of non-stationary signals because FrFT is unified in the time-frequency plane [10]. Some basic properties of FrFT are listed below for our presentation.

(1) Boundedness. The relationship between FrFT and FT is as follows:

$$\mathcal{F}^\alpha\{f(t)\}(u)=\sqrt{2\pi}A_\alpha e^{j\frac{u^2}{2}\cot\alpha}\cdot\mathcal{F}\left[f(t)e^{j\frac{t^2}{2}\cot\alpha}\right](u\csc\alpha), \tag{4}$$

where $\mathcal{F}$ is the integer order Fourier transform operator. $\mathcal{F}^\alpha\{f(t)\}(u)=\mathcal{F}[f(t)]$ when $\alpha=2n\pi+\frac{\pi}{2}$. $\mathcal{F}^\alpha$ is an identity operation when $\alpha=2n\pi$ [27].
(2) Additivity. $\mathcal{F}^{\alpha_1}\mathcal{F}^{\alpha_2}=\mathcal{F}^{\alpha_1+\alpha_2}$.
(3) Fractional Fourier convolution [28].

$$z(t)=x(t)\overset{\alpha}{*}h(t)=e^{-j\frac{t^2}{2}\cot\alpha}\left[\left(x(t)e^{j\frac{t^2}{2}\cot\alpha}\right)*h(t)\right], \tag{5}$$

where $\overset{\alpha}{*}$ denotes the fractional convolution operator. $*$ denotes the traditional convolution operator. The FrFT of $z(t)$ can be denoted as follows:

$$Z_\alpha(u)=\sqrt{2\pi}X_\alpha(u)H(u\csc\alpha). \tag{6}$$

2.2. Fractional bandpass signal and its sampling theorems

A fractional bandpass signal $f(t)$ satisfies that its energy is finite. The FrFT of $f(t)$ is zero outside the region $(-\Omega_0-\Omega_\alpha,-\Omega_0+\Omega_\alpha)\cup(\Omega_0-\Omega_\alpha,\Omega_0+\Omega_\alpha)$.

$$F_\alpha(u)=0,\ \text{ for } |u|\geq(\Omega_0+\Omega_\alpha)\ \text{ and }\ |u|\leq(\Omega_0-\Omega_\alpha),\ \Omega_0\geq\Omega_\alpha, \tag{7}$$

where $2\Omega_\alpha$ is the fractional bandwidth of $f(t)$. $\Omega_h=\Omega_0+\Omega_\alpha$, and $\Omega_l=\Omega_0-\Omega_\alpha$. According to Parseval's theorem, the bandlimited signal can also be expressed as:

$$\int_{-\infty}^{+\infty}|f(t)|^2\mathrm{d}t=\int_{-\Omega_h}^{-\Omega_l}|F_\alpha(u)|^2\mathrm{d}u+\int_{\Omega_l}^{\Omega_h}|F_\alpha(u)|^2\mathrm{d}u<\infty.$$

Sampling and reconstruction in the FrFD can be viewed as an orthogonal projection of a signal onto a subspace of fractional bandlimited signals. Xia [11] noted that if a nonzero signal $f(t)$ is bandlimited with angle α, then $f(t)$ cannot be bandlimited with another angle β, where $\beta\neq\alpha+n\pi$ for any integer n.

Suppose that the carrier Ω_0 is unknown; the sampling rate would thus be $T_s=\pi\sin\alpha/(\Omega_0+\Omega_\alpha)$ to avoid spectrum aliasing. In other words, the rate of the analog-to-digital converter depends on the maximum fractional "frequency" of the signal. The sampling rate must also be no less than $\Omega_h/(\pi\sin\alpha)$ when the signal is bandlimited within the region (Ω_l,Ω_h). The sampling rate is difficult to realize when Ω_0 is very large. If the carrier is known, then the sampling rate can be reduced by multiplying the original signal with the carrier [29]. $f(t)$ can be restored as:

$$f(t)=\sqrt{\frac{1+j\cot\alpha}{2\pi}}e^{-\frac{j}{2}t^2\cot\alpha}\sum_{n=-\infty}^{+\infty}f(nT_s)e^{\frac{j}{2}(nT_s)^2\cot\alpha}\times\frac{\sin[(t-nT_s)\Omega_\alpha\csc\alpha]}{(t-nT_s)\Omega_\alpha\csc\alpha}\times e^{j\Omega_0\csc\alpha(t-nT_s)}, \tag{8}$$

where the sampling rate $\frac{1}{T_s}=\Omega_\alpha/(\pi\sin\alpha)$ is twice the bandwidth of $f(t)$.

For a low-frequency narrowband signal with $\Omega_l=0$, $\Omega_h=\Omega_\alpha$, Eq. (8) will reduce to the well-known sampling theorem [11].

$$f(t)=\sqrt{\frac{1+j\cot\alpha}{2\pi}}e^{-\frac{j}{2}t^2\cot\alpha}\sum_{n=-\infty}^{+\infty}f(nT_s)\times e^{\frac{j}{2}(nT_s)^2\cot\alpha}\times\frac{\sin[(t-nT_s)\Omega_\alpha\csc\alpha]}{(t-nT_s)\Omega_\alpha\csc\alpha}. \tag{9}$$

Fractional Fourier series (FrFS) are a generalization of Fourier series [25]. FrFS will converge to FrFT when the computing interval T approaches infinity. FrFS is denoted by:

$$f(t)=\sum_{n=-\infty}^{\infty}C_{\alpha,n}\sqrt{\frac{\sin\alpha+j\cos\alpha}{T}}\cdot e^{-\frac{j}{2}\left(t^2+\left(n\frac{2\pi}{T}\sin\alpha\right)^2\right)\cot\alpha+jnt\frac{2\pi}{T}}, \tag{10}$$

where $C_{\alpha,n}$ is the coefficient of the FrFS expansion. The coefficients of the FrFS expansion are computed by the inner product of the signal and chirp basis signals.

$$C_{\alpha,n}=\sqrt{\frac{\sin\alpha-j\cos\alpha}{T}}\int_{-T/2}^{T/2}f(t)\cdot e^{\frac{j}{2}(t^2+(n\frac{2\pi}{T}\sin\alpha)^2)\cot\alpha-jnt\frac{2\pi}{T}}\mathrm{d}t. \tag{11}$$

2.3. Modulated wideband converter

Mishali et al. presented a multichannel parallel modulated and sampled architecture called the *modulated wideband converter* (MWC) [21], which is composed of a bank of modulators, low-pass filters and ADCs. The MWC is effective for the sparse signal in FD. A block diagram of the MWC system is presented in Fig. 1.

The signal $x(t)$ is sent in parallel to m mixing channels, being multiplied in each channel by a different periodic repeating pattern of M random equiprobable sign values. The sign vector $p_i(t)=[s_{i,0},s_{i,1},\ldots,s_{i,M-1}]$ with $s_{i,k}\in\{-1,1\}$. The index $i=1,2,\ldots,m$ identifies the mixing channel. The sign vectors are assumed to be mutually uncorrelated with $E[p_i^T(t),p_j(t)]=0$ for $i\neq j$. $E[\cdot]$ denotes the statistical expectation operator, which refers to the probability of

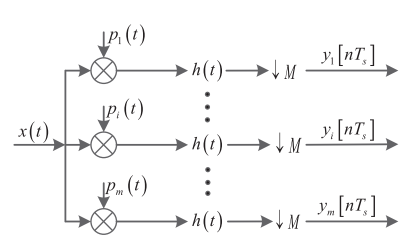

Fig. 1. Structure of the modulated wideband converter.

sign values. For simplicity, suppose that the observation interval of $x(t)$ is P periods of the modulating sign pattern such that the signal length can be expressed as $N = P{\cdot}M$. After mixing, the signals are low-pass filtered and downsampled by a decimation factor M. The amount of data at the MWC outputs is thus reduced from N=MP samples in a single vector to a measurement matrix with size mP. The ratio M/m is called the compression factor. The system has three stages:

(1) Mixing and sub-Nyquist downsampling. It is an important implementation of the MWC concept that allows compressive acquisition of sparse wideband signals at sub-Nyquist rates. The sampling sequence $y(f) = \mathbf{A}z(f)$, where $\mathbf{A}$ is the sensing matrix. The ith vector A_i is the coefficient of the DFT of the $p_i(t)$ vector.
(2) Finite support recovery. It is based on the recovery of jointly sparse vectors. $y(f) = \mathbf{A}z(f)$ is rewritten in the discrete frequency domain as $y_i(n) = \sum_{l=-L_0}^{+L_0} \theta_{il} x_l(n)$ where $x_l(n)$ is the sampling sequence of the lth spectrum slice of $x(t)$ and A_{il} is the entries of $\mathbf{A}$. It is easy to prove that $\mathbf{A}$ satisfies the restricted isometry property (RIP) [30]. The reconstruction of unknown sparse vectors $x_l(n)$ could be cast as the multiple measurement vector (MMV) problem, which could be resolved by joint recovery.
(3) Signal recovery is realized by simple inversion of the linear measurement equation restricted to active sub-bands.

The MWC system is constructed based on the sparsity of the multiband signals. Most of the system parameters depend on the maximum bandwidth of the signals. Occasionally, the signal is sparse in the FrFD rather than in the FD, and even if the signals satisfy the condition of the MWC, the maximum bandwidth of signals in the FD is considerably wider than the bandwidth in the FrFD. Although the classic MWC can sample and reconstruct such signals that show better sparsity in the FrFD such as the signals in Fig. 2, the probability of successful recovery is low even with many hardware resources. It is not economical to use the classic MWC to sample the signals that are more sparse in the FrFD.

3. Compressed sampling for multiband signals in the FrFD

3.1. Problem formulation

An example for the sparsity of fractional multiband signals is shown in Fig. 2. In this figure, “FT” and “FrFT” are the Fourier transform and fractional Fourier transform of the “signals” respectively. It is observed that the signal has better sparsity in the FrFD than in the traditional FD. As we know, the narrower the nonzero part of the available spectrum is, the better property the spectrum has.

In most practical applications, the signals of interest are sparse in a certain domain, which typically occupy only a few among several

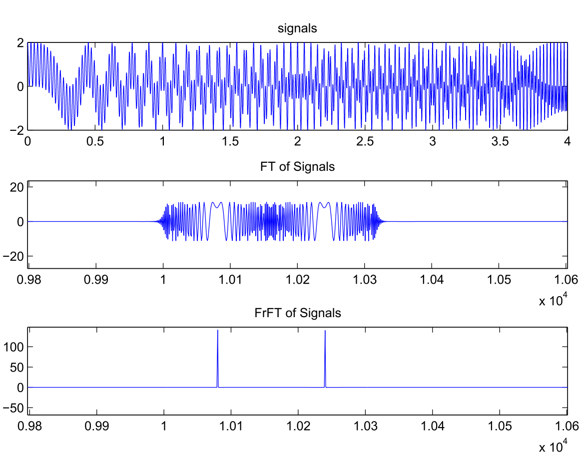

Fig. 2. Illustration of the sparsity of fractional multiband signals.

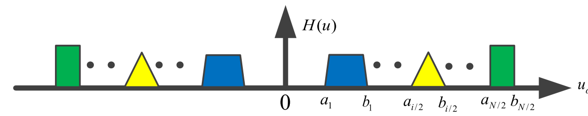

Fig. 3. Illustration of a multiband signal in αth-order FrFT domain.

possible bands, for example, spectrum sensing and wireless communications. In Fig. 3, a sparse multiband signal in the αth FrFD contains N nonzero narrow fractional Fourier bandlimited signals. The spectral positions of the narrow fractional bandlimited signals are random and unknown. The valid fractional “frequency” components of signal $f(t)$ are the set of non-zero spectrum. The maximum spectral width of the signal is $B_\alpha = \max(b_i - a_i)$, $i \in [1, N/2]$. $2B_\alpha \csc\alpha$ is considered to be the minimum sampling frequency for the multiband signal according to information theory [11,31]. N is even due to the conjugate symmetry of the signal. The sampling method for the multiband signal is to construct the relationship between the sampling rate and the maximum width of the signal. A high sampling rate is not necessary until a compressed sampling method for fractional Fourier bandlimited signals is proposed.

3.2. System description

Roughly speaking, our proposal is based on two points. First, a frequency shifting does not have any impact on the signal's fractional bandlimited order. Second, a signal is occasionally sparse in the αth-order FrFD rather than in the FD; in other words, one signal is bandlimited or sparse in some FrFD but not both. The α-bandlimited signal could be compressively sampled with a digital structure, which is similar to the classic MWC. The structure of our proposed fractional Fourier MWC system is shown in Fig. 4. There are two mixing steps. The first mixing is to establish the relationship between FrFT and FT. The spectrum of the mixed product is aliased by the random modulation at the second step. At the first mixing, we multiply $\exp(\frac{j}{2}t^2\cot\alpha)$ with the original signal, and then the product is mixed with the random sign signal. The production of the mixing signal is filtered by a low-pass filter, and then it is sampled and reconstructed by the orthogonal matching pursuit. The final result can be recovered by multiplying the reconstructed signal by $\exp(-\frac{j}{2}t^2\cot\alpha)$. Because the feature that the α-bandlimited signal is sparse at the αth-order FrFT, it is easy to recover the input signal from the FrFD. It is clear that the classic MWC is a special case at $\alpha = \frac{\pi}{2}$.

3.3. Fractional Fourier transform domain analysis

In this part, we derive the relationship between the unknown signal $x(t)$ and sampling sequences $\tilde{y}_i(n)$. Specifically, $x(t)$ is input to m channels simultaneously. We take the ith channel as an example to explain how every channel works. The system only requires $p_i(t)$ to be periodic; thus, $p_i(t)$ is selected as a sign function for each of M equal intervals as the follows:

$$p_i(t) = s_{ik},\ k\frac{T_p}{M} \le t \le (k+1)\frac{T_p}{M},\ 0 \le k \le M-1, \tag{12}$$

where $s_{ik} \in \{+1, -1\}$ and $p_i(t)$ is a periodic function with period T_p.

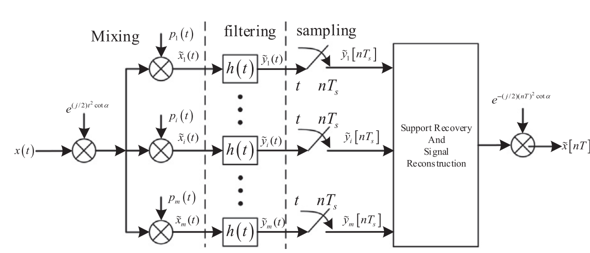

Fig. 4. Multichannel compressed sampling method in the FrFD.

The FrFS of $e^{-j\frac{t^2}{2}\cot\alpha}p_i(t)$ is denoted by:

$$e^{-j\frac{t^2}{2}\cot\alpha}p_i(t)=\sum_{l=-\infty}^{\infty}C_{\alpha,il}\sqrt{\frac{\sin\alpha+j\cos\alpha}{T}}\cdot e^{-\frac{j}{2}\left(t^2+\left(l\frac{2\pi}{T}\sin\alpha\right)^2\right)\cot\alpha+jlt\frac{2\pi}{T}},\tag{13}$$

where T is the time duration. $C_{\alpha,il}$ is the coefficient of the FrFS expansion with the transform angle α. The FrFS coefficients are computed by the inner product of the signal and chirp basis which is denoted by the following:

$$C_{\alpha,il}=\sqrt{\frac{\sin\alpha-j\cos\alpha}{T}}\int_{-T/2}^{T/2}p_i(t)e^{-j\frac{t^2}{2}\cot\alpha}\cdot e^{\frac{j}{2}(t^2+(l\frac{2\pi}{T}\sin\alpha)^2)\cot\alpha-jlt\frac{2\pi}{T}}\mathrm{d}t.\tag{14}$$

The mixed product signal and its FT can be denoted by:

$$\begin{aligned}\tilde{y}_i(t)&=\left(x(t)p_i(t)e^{\frac{j}{2}t^2\cot\alpha}\right)*h(t),\ \mathcal{F}(\tilde{y}_i(t))(u\csc\alpha)\\&=\sqrt{2\pi}\mathcal{F}\left(x(t)p_i(t)e^{\frac{j}{2}t^2\cot\alpha}\right)(u\csc\alpha)\times H(u\csc\alpha),\end{aligned}\tag{15}$$

where $\mathcal{F}\left(x(t)p_i(t)e^{\frac{j}{2}t^2\cot\alpha}\right)(u\csc\alpha)$ is computed as:

$$\mathcal{F}\left(x(t)p_i(t)e^{\frac{j}{2}t^2\cot\alpha}\right)(u\csc\alpha)=\mathcal{F}\left(x(t)(p_i(t)e^{-\frac{j}{2}t^2\cot\alpha})e^{jt^2\cot\alpha}\right)(u\csc\alpha).\tag{16}$$

Substitute the FrFS of the $e^{-j\frac{t^2}{2}\cot\alpha}p_i(t)$ into (16),

$$\begin{aligned}&\mathcal{F}\left(x(t)(p_i(t)e^{-\frac{j}{2}t^2\cot\alpha})e^{jt^2\cot\alpha}\right)(u\csc\alpha\\&\backslash)=\int_{-\infty}^{+\infty}x(t)\left(\sum_{l=-\infty}^{\infty}C_{\alpha,il}\sqrt{\frac{\sin\alpha+j\cos\alpha}{T}}e^{-\frac{j}{2}(t^2+(l\frac{2\pi}{T}\sin\alpha)^2)\cot\alpha+jlt\frac{2\pi}{T}}\right)\\&\times e^{jt^2\cot\alpha-jtu\csc\alpha}\mathrm{d}t=\sqrt{\frac{\sin\alpha+j\cos\alpha}{T}}\sum_{l=-\infty}^{\infty}C_{\alpha,il}\\&\times e^{-\frac{j}{2}(l\frac{2\pi}{T}\sin\alpha)^2\cot\alpha}\int_{-\infty}^{+\infty}x(t)e^{\frac{j}{2}t^2\cot\alpha-jt\csc\alpha(u-\frac{2\pi l}{T_p}\sin\alpha)}\mathrm{d}t\\&=\frac{1}{A_\alpha}\sum_{l=-\infty}^{\infty}\sqrt{\frac{\sin\alpha+j\cos\alpha}{T}}C_{\alpha,il}e^{-\frac{j}{2}(l\frac{2\pi}{T}\sin\alpha)^2\cot\alpha}e^{-\frac{j}{2}(u-\frac{2\pi l\sin\alpha}{T_p})^2\cot\alpha}\mathcal{X}_\alpha\\&\times(u-\frac{2\pi l\sin\alpha}{T_p})=\frac{1}{A_\alpha}\sum_{l=-\infty}^{\infty}c_{il}e^{-\frac{j}{2}(u-\frac{2\pi l\sin\alpha}{T_p})^2\cot\alpha}\mathcal{X}_\alpha\left(u-\frac{2\pi l\sin\alpha}{T_p}\right),\end{aligned}\tag{17}$$

where $\mathcal{X}_\alpha(u)$ is the FrFT of $x(t)$. It is a bandlimited signal with the maximum bandwidth not exceeding B_α. $c_{il}=\sqrt{\frac{\sin\alpha+j\cos\alpha}{T}}C_{\alpha,il}e^{-\frac{j}{2}(l\frac{2\pi}{T}\sin\alpha)^2\cot\alpha}$. The two-step mixing simply produces a scale transformation and a fractional "frequency" shifting in Eq. (17). $\exp(-\frac{j}{2}(u-\frac{2\pi l\sin\alpha}{T_p})^2\cot\alpha)\mathcal{X}_\alpha(u-\frac{2\pi l\sin\alpha}{T_p})$ is also a bandlimited signal with the maximum bandwidth B_α and a relative $\frac{2\pi l\sin\alpha}{T_p}$ shift in the FrFD.

The mixing product is truncated by a low-pass filter with cutoff u_s, where u_s is the fractional sampling rate for each channel. Consider $h(t)$ to be an ideal rectangular function in the FrFD and serves as a preceding anti-aliasing filter. If the sampling rate is chosen to be $u_s=B_\alpha$, then $f_s=u_s\csc\alpha$. The low-pass filter $H(u\csc\alpha)=1$, $u\in[-\frac{B_\alpha}{2},\frac{B_\alpha}{2}]$; otherwise, $H(u\csc\alpha)=0$, as Fig. 5, $h(t)=\mathrm{sinc}(B_\alpha\csc\alpha/2)$. Substituting Eq. (17) into Eq. (15), $\mathcal{F}(\tilde{y}_i(t))$ can be simplified as:

$$\mathcal{F}(\tilde{y}_i(t))=\sum_{l=-L_0}^{L_0}c_{il}e^{-\frac{j}{2}(u-\frac{2\pi l\sin\alpha}{T_p})^2\cot\alpha}\mathcal{X}_\alpha\left(u-\frac{2\pi l\sin\alpha}{T_p}\right),\tag{18}$$

where the spectrum of $\mathcal{F}(\tilde{y}_i(t))$ is the repetition of the spectrum of $e^{-\frac{j}{2}u^2\cot\alpha}\mathcal{X}_\alpha(u)$. L_0 is chosen as the smallest integer such that it must cover all nonzero spectrum slices of $\exp(-\frac{j}{2}u^2\cot\alpha)\mathcal{X}_\alpha(u)$. The exact

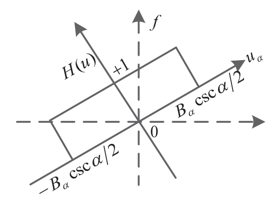

Fig. 5. Low-pass filter $h(t)$ in the FD.

value of L_0 is calculated by:

$$-\frac{u_s}{2}+(L_0+1)u_p\geq\frac{u_{NYQ}}{2}\rightarrow L_0=\left[\frac{u_{NYQ}+u_s}{2u_p}\right]-1,\tag{19}$$

where u_s is the fractional sampling rate. $u_p=\frac{2\pi\sin\alpha}{T_p}$ is the fractional "frequency" of the mixing signal $p_i(t)$. The fractional Nyquist sampling rate is $u_{NYQ}=2b_{N/2}$ when the maximum fractional Fourier "frequency" of the signal is $b_{N/2}$. $L_0=(b_{N/2}+u_s)\csc\alpha/(2f_p)-1$. We choose the frequency of the sign matrix signal $u_p\geq B_\alpha$. The sampling rate $u_s=u_p\geq B_\alpha$. The number of spectrum slices is $L=2L_0+1$.

$C_{\alpha,il}$ is the FrFS coefficient of $\exp(-\frac{j}{2}t^2\cot\alpha)p_i(t)$ where $p_i(t)$ is a periodic function. $c_{il}=\sqrt{\frac{\sin\alpha+j\cos\alpha}{T}}\exp(-\frac{j}{2}(\frac{2\pi l\sin\alpha}{T_p})^2\cot\alpha)C_{\alpha,il}$ is denoted as follows:

$$\begin{aligned}\sqrt{\frac{\sin\alpha+j\cos\alpha}{T}}e^{-\frac{j}{2}(\frac{2\pi l}{T}\sin\alpha)^2\cot\alpha}C_{\alpha,il}&=\frac{1}{T}\int_0^{T_p}p_i(t)e^{-\frac{j}{2}t^2\cot\alpha}e^{\frac{j}{2}t^2\cot\alpha-jlt\frac{2\pi}{T_p}}\mathrm{d}t\\&=\frac{1}{T}\int_0^{T}\sum_{k=0}^{M-1}a_{il}e^{-jlk\frac{2\pi}{M}}\int_0^{\frac{T_p}{M}}e^{-jlt\frac{2\pi}{T_p}}\mathrm{d}t,\end{aligned}\tag{20}$$

where T is the time duration which is an integral multiple of T_p. Eq. (20) reduces to the following:

$$\sqrt{\frac{\sin\alpha+j\cos\alpha}{T}}e^{-\frac{j}{2}(\frac{2\pi l}{T}\sin\alpha)^2\cot\alpha}C_{\alpha,il}=\frac{1}{T_p}\int_0^{T_p}\sum_{k=0}^{M-1}a_{il}e^{-jlk\frac{2\pi}{M}}\int_0^{\frac{T_p}{M}}e^{-jlt\frac{2\pi}{T_p}}\mathrm{d}t.\tag{21}$$

Let $\bar{\mathbf{F}}$ be an $M\times M$ discrete Fourier transform (DFT) matrix. The ith column is denoted by:

$$\bar{\mathbf{F}}_i=[\theta^{0i},\theta^{1i},\ldots,\theta^{(M-1)i}]^T,\quad i\in[0,M-1].\tag{22}$$

Let $\mathbf{F}=[\bar{\mathbf{F}}_{L_0},\ldots,\bar{\mathbf{F}}_{-L_0}]$ be $M\times L$ matrix which is a column subset of $\bar{\mathbf{F}}$. To guarantee no distortion of the original signal's spectrum, set M=L. Let $\mathbf{S}$ be the $m\times M$ sign matrix with ith row and kth column element s_{ik}. $\mathbf{D}=diag(d_{L_0},\ldots,d_{-L_0})$ is an $L\times L$ diagonal matrix with d_l defined by the following:

$$d_l=\frac{1}{T_p}\int_0^{\frac{T_p}{M}}e^{-j\frac{2\pi}{p}lt}\mathrm{d}t=\begin{cases}\dfrac{1}{M}, & l=0,\\ \dfrac{1-\theta^l}{2j\pi l}, & l\neq 0,\end{cases}\tag{23}$$

where $\theta=e^{-j2\pi/M}$. The output $\mathbf{y}_\alpha(u)$ is given by:

$$\mathbf{y}_\alpha(u)=\mathbf{SFD}\mathbf{z}(u),\tag{24}$$

where $z(u)=g(u)x_\alpha(u)$, $\mathbf{x}_\alpha(u)=[\mathcal{X}_\alpha(u-L_0u_p),\ldots,\mathcal{X}_\alpha(u),\ldots,\mathcal{X}_\alpha(u+L_0u_p)]^T$. $\mathbf{g}(u)=\mathrm{diag}[g_{L_0},\ldots,g_{-L_0}]$, where $g_l=\exp(-\frac{j}{2}(u-lu_p)^2\cot\alpha)$. $\mathbf{A}=\mathbf{SFD}$ is termed as the sensing matrix. The final expression is provided in Eq. (25).

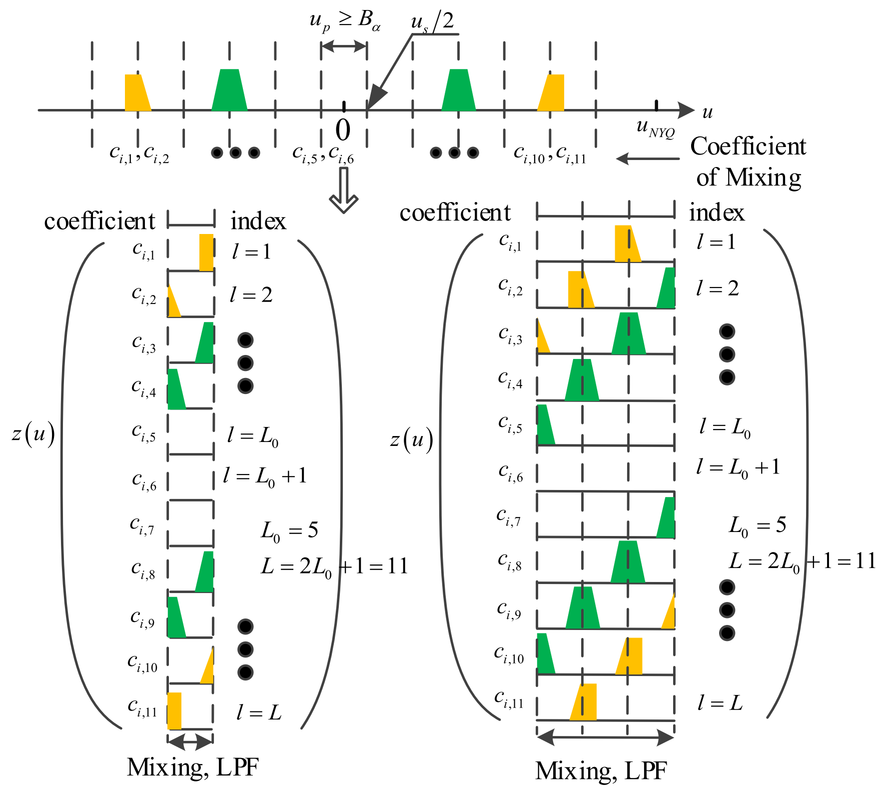

Fig. 6. Relationship between sparse representation and spectrum of signal.

$$\begin{pmatrix} y_{\alpha,1}(u) \\ y_{\alpha,2}(u) \\ \vdots \\ y_{\alpha,m}(u) \end{pmatrix} = \begin{bmatrix} s_{1,0} & \cdots & s_{1,M-1} \\ \vdots & \ddots & \vdots \\ s_{m,0} & \cdots & s_{m,M-1} \end{bmatrix} \begin{bmatrix} | & \cdots & | & \cdots & | \\ F_{L_0} & \cdots & F_0 & \cdots & F_{-L_0} \\ | & \cdots & | & \cdots & | \end{bmatrix}$$
$$\times \begin{bmatrix} d_{L_0} & & \\ & \ddots & \\ & & d_{-L_0} \end{bmatrix} \begin{pmatrix} e^{-\frac{j}{2}(u-L_0u_p)^2\cot\alpha}X_\alpha(u-L_0u_p) \\ \vdots \\ e^{-\frac{j}{2}u^2\cot\alpha}X_\alpha(u) \\ \vdots \\ e^{-\frac{j}{2}(u+L_0u_p)^2\cot\alpha}X_\alpha(u+L_0u_p) \end{pmatrix}. \tag{25}$$

Fig. 6 illustrates how the proposed system works. The system implicitly applies a grid on the fractional "frequency" axis, which divides a partition of the spectrum into M equal-width sub-bands. Consider the symmetry of the real signal spectrum. There are 4 limited bands when the number of input bandlimited signals is 2. The spectrum slices are moved to the baseband with the coefficient c_{ij}. To provide a clear relationship between the result $y_\alpha(u)$ and the support set $z(u)$ in the ith channel, the figure separates the spectrum slices into vertical panes. In the real system, all of the spectrum slices alias together in the ith channel. Each entry of $z(u)$ is a slice of $y_\alpha(u)$ whose length is u_s. In the left half plane, $u_s = u_p \approx B_\alpha$, and thus, the number of spectrum slices is L=11. In the right half plane, $u_s = 3u_p \approx 3B_\alpha$, L=11. It is clear that the right plane can be divided into three similar channels. There is a tradeoff between the number of channels and every channel's sampling rate, in which a higher sampling rate corresponding to more channels.

3.4. Choice of parameters and recovery

The best parameters need to be chosen, such as the number of channels m and the sampling rate $u_s = 2\pi/T_s \sin\alpha$. To make each band only contribute to a continuous nonzero sequence $z(u)$, we choose the sign matrix signal $u_p \geq B_\alpha$, which means that $f_p \geq B_\alpha \csc\alpha$, $T_p \leq \frac{2\pi\sin\alpha}{B_\alpha}$. Each channel's sampling rate u_s is set as $u_s \geq u_p$ to keep every slice of the spectrum sampled under the Nyquist law. The number of channels m and the sampling rate of a single channel determine the system's sampling rate mu_s. The number of channels, every channel's sampling rate and the frequency of the mixing sign signal need to satisfy $mu_s \geq 2Nu_p$ such that the sampling data can cover the least width of the spectrum and $M \geq \frac{u_{NYQ}}{u_p}$. In practical applications, the hardware is unalterable once produced. A sufficient number of channels allows to the signal to be easily recovered considering the burden of the hardware. There is a tradeoff among the hardware costs, number of channels and sampling rate of every channel.

$z(u)$ is partly composed by $\boldsymbol{x}_\alpha(u)$ in Eq. (24); thus, the recovery of the original signal $x(t)$ directly is almost impossible, but it could be changed to be the recovery of the spectrum of $x(t)e^{\frac{j}{2}t^2\cot\alpha}$. The system falls into the problem of sparse solutions [32]. The reconstruction method for the multiband signals is specified in [21]. The problem is converted to develop an adaptive reconstruction algorithm for signals with unknown spectral occupation. The reconstruction could be divided into two stages: spectral support estimation in the FrFD and signal reconstruction in the time domain. The digital computations of the recovery support are grouped by a continuous to finite (CTF) block. One of the elements of the CTF is to solve a multiple measurement vectors (MMV) problem, which is an uncertain linear system for the sparest solution matrices. We rewrite Eq. (18) in the discrete fractional Fourier domain as:

$$y_{\alpha,i}(n) = \sum_{l=-L_0}^{+L_0} c_{il} z_{\alpha,l}(n), \tag{26}$$

where $z_{\alpha,l}(n)$ is the sampling sequence of the lth fractional spectrum slice of $x(t)e^{\frac{j}{2}t^2\cot\alpha}$ and c_{il} are the entries of the sensing matrix $\mathbf{A}$.

The goal is to find $z(n) = [z_{\alpha,1}(n), z_{\alpha,2}(n), \ldots, z_{\alpha,m}(n)]$ with as few nonzero rows as possible. Let $\mathbf{U}$ denote the index set that marks the position of the nonzero elements of $z(n)$. The expression of the support basis can be denoted by:

$$\mathbf{U} = \bigcup I(z(n)). \tag{27}$$

Reconstruction of the signal $x(t)\exp(j2\pi t^2\cot\alpha)$ can be achieved by finding $\mathbf{U}$. If the index set of $z(n)$ satisfies $\mathbf{U} = \mathrm{rank}(\mathbf{A})$, then it is a perfect reconstruction. As long as the mixing function $p_i(t)$ is generated randomly, the system satisfies the condition of the reconstruction. It is achievable to recover the sparsity basis $\exp(-\frac{j}{2}(u - \frac{2\pi l\sin\alpha}{T_p})^2\cot\alpha)\mathcal{X}_\alpha(u - \frac{2\pi l\sin\alpha}{T_p})$ by the orthogonal matching pursuit (OMP). $e^{\frac{j}{2}(nT)^2\cot\alpha}x(nT)$ is recovered by inversion of the linear measurement equation in the time domain. The original signal could be recovered by multiplying $e^{-\frac{j}{2}(nT)^2\cot\alpha}$.

3.5. Influence of the fractional order

The αth-order FrFT is equivalent to rotating the signal in the clockwise direction with angle α. Whereas FrFT can be regarded as the projection on the rotated frequency axis u, the bandwidth of the signal directly depends on the order of the FrFT. Suppose that

$$\mathcal{X}_\alpha(u) = 0, \quad u > |u_\alpha|, \tag{28a}$$

$$\mathcal{X}_\beta(v) = 0, \quad v > |v_\beta|, \tag{28b}$$

where $\mathcal{X}_\alpha(u)$ and $\mathcal{X}_\beta(v)$ are αth-order and βth-order FrFTs of $x(t)$, respectively. $|\beta - \alpha| = \Delta\alpha$, and the error $\Delta\alpha$ between α and β can be interpreted as the error between the real order and its theoretical value. $\Delta\alpha$ has some effect on the width of the fractional Fourier band.

$$\mathcal{F}^\beta[x(t)](v) = \mathcal{F}^{\pm\Delta\alpha}\{\mathcal{F}^\alpha[x(t)]\}(v) = \mathcal{F}^{\pm\Delta\alpha}\{\mathcal{X}_\alpha(u)\}(v). \tag{29}$$

Substitute the definition of the FrFT into Eq. (29).

$$\begin{aligned}\mathcal{F}^{\Delta\alpha}\{\mathcal{X}_\alpha(u)\}(v) = &\int_{-u_\alpha}^{u_\alpha}\int_{-v_\beta}^{v_\beta}\mathcal{X}_\beta(u')K_{-\Delta\alpha}(u', u)\mathrm{d}u' K_{\Delta\alpha}(u, v)\\ &\times \mathrm{d}u = \lambda_{\Delta\alpha}^*(u)\int_{-v_\beta}^{v_\beta}\mathcal{X}_\beta(u')\lambda_{\Delta\alpha}(u')\\ &\frac{\sin(u_\alpha(u-u')\csc\Delta\alpha)}{\pi(u-u')}\mathrm{d}u' = \mathcal{X}_\beta(u)\overset{\Delta\alpha}{*}\frac{\sin(u_\alpha u\csc(\Delta\alpha))}{\pi u},\end{aligned} \tag{30}$$

where $\mathcal{F}$ is the FT operator. $\overset{\Delta\alpha}{*}$ is the fractional convolution operator defined by Eq. (5).

$x(t)$ will not be bandlimited with the β FrFT in the same domain $[-u_\alpha, u_\alpha]$. If $\beta = \frac{\pi}{2}$, then $\mathcal{F}^\beta\{x(t)\}(v) = \frac{1}{2\pi}\mathcal{X}_\alpha(v\sin\alpha)e^{-j\frac{1}{2}v^2\sin\alpha\cos\alpha}$, which is bandlimited in $[-u_\alpha\csc\alpha, u_\alpha\csc\alpha]$. The error of the fractional order will lead to the variation of the bandwidth. The variation may lead to a spectrum aliasing for the multiband signal in the FrFD. This bandwidth of signal in two arbitrary fractional domains cannot be the same simultaneously. It is difficult to obtain the real bandwidth, which depends the property of the signal. Roughly speaking, the larger the error of FrFT order, the more uncertainty there will be in reconstruction. The chirp signal is taken as an example to show how the $\Delta\alpha$ affects the bandwidth.

$$s(t) = A_i\mathrm{rect}\left(\frac{t-\tau_i}{T_i}\right)e^{j2\pi\theta_1 t + j\pi\theta_2 t^2}. \tag{31}$$

The spectrum section that signal $s(t)$ occupies in the FrFD is $\left[\theta_{i1}\sin\alpha_i - \frac{2\pi}{T_i}|\sin\alpha_i|, \theta_{i1}\sin\alpha_i + \frac{2\pi}{T_i}|\sin\alpha_i|\right]$ when $\theta_2 = -\cot\alpha$. The bandwidth in the FrFD is $4\pi\sin\alpha/T_i$. The bandwidth of signal $s(t)$ at order β where $\beta \neq \alpha$ can be computed as:

$$\begin{aligned}F^\beta[s(t)](u) = &\int_{-\infty}^{\infty}K_\beta(t, u)s(t)\mathrm{d}t = A_\beta e^{j\pi u^2\cot\beta}\\ &\times\int_0^T e^{j\pi t^2(\cot\beta+\theta_2) - j2\pi t(u\csc\beta+\theta_1)}\mathrm{d}t.\end{aligned} \tag{32}$$

The formula can be interpreted as the FT of $e^{j\pi t^2(\cot\beta+\theta_2)}$, which occupies the bandwidth of $(\cot\beta + \theta_2)T$. The result is also verified by rotating in Fig. 7. The thick red line presents the time-frequency distribution line of the signal $s(t)$. β_1 and β_2 are the angles of the FrFT. The $u\perp v$ means that there is a minimum bandwidth. The signal has the best sparsity in the u domain. The maximum spectrum amplitude of the signal is $\frac{A}{\sqrt{\theta_2}}$ when $\theta_2 = -\cot\beta$. The spectrum section that the signal occupies in the FD is $[\theta_1 - \frac{T}{2}\theta_2, \theta_1 + \frac{T}{2}\theta_2]$. The spectrum section that signal $s(t)$ occupies in the FrFD is $[\theta_1\sin\alpha - \frac{T}{2}\theta_2|\sin\alpha|, \theta_1\sin\alpha + \frac{T}{2}\theta_2|\sin\alpha|]$. The best order α will tend to zero as the modulated rate θ_2 increases, and a slight error will lead to large changes of bandwidth. From the above analysis, the chirp signal has the best energy accumulation property in the corresponding order FrFD and has a flat spectrum in the FrFD of other orders.

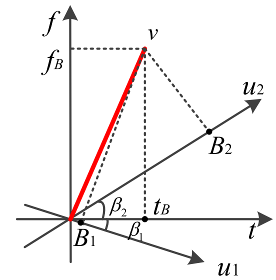

Fig. 7. Bandwidth of chirp signals with different fractional orders.

4. Numerical simulation

4.1. Design of simulation

To evaluate the performance of the proposed method, we use the chirp signal as the test subject, which is a typical fractional Fourier bandlimited signal. We simulate the system on the test subject contaminated by zero-mean Gaussian noise. The original multiband signal is denoted by $x(t)$. The noisy signal is $x(t) + n(t)$, where $n(t)$ is white Gaussian noise. The SNR (signal-to-noise ratio) is defined by $10\log(\|x\|^2/\|n\|)$. $x(t)$ is given by the following:

$$x(t) = \sum_{i=1}^{N/2}x_i(t) = \sum_{i=1}^{N/2}E_i\mathrm{rect}\left(\frac{t-\tau_i}{s_i}\right)e^{j2\pi B_i t^2}\cos(2\pi f_i t), \tag{33}$$

where $x_i(\cdot)$ is the ith original signal. N represents the number of active bands. Suppose the symmetry of the real signal spectrum, where $N/2$ is the number of signals. E_i is the amplitude of the signal which could be random or fixed. B_i is the signal modulation rate $B_i = \{0.190, 0.194, 0.198, 0.200\} \times 10^9$. s_i is the time scale factor which determines the signal duration. Let $B_i s_i \le 10$ M, which means that the bandwidth in the FD does not exceed 10 MHz, with $s_i = \{0.05, 0.05, 0.05, 0.05\}$ for convenience. τ_i is the time delay between different signals which is selected randomly. f_i is a random frequency carrier. The bandlimited order $\alpha = -0.5 \times 10^{-8}$. $\mathrm{rect}(\cdot)$ is a rectangular time-window denoted by $\mathrm{rect}(t) = 0$, if $|t| > \frac{1}{2}$; else, $\mathrm{rect}(t) = 1$. The signal is both frequency bandlimited and fractional bandlimited with different bandwidths in the observation interval. The choices of the parameters are listed in Table 1.

Simultaneous orthogonal matching pursuit (SOMP) [33] is applied in the system, which is fast and easy to implement for engineers to construct signals in the simulations. The normalized mean squared error (NMSE) and successful recovery probability are used to measure the performance of the compressed sampling. Successful recovery probability is defined as the ratio of the number of empirical successful reconstructions and total trials. Successful recovery is defined when the estimated support set is equal to the true support. Obviously, the greater the successful recovery probability is, the better the performance is. NMSE is defined as:

Table 1
Choices of parameters for multiband sampling.

FD	FrFD	Meaning
N: 4,6,8	N: 4,6,8	Number of sparse bands N
B: 10 MHz	$B_\alpha \csc\alpha$: 0.5 MHz	Maximum bandwidth of the active bands
f_{NYQ}: 1 GHz	$u_{NYQ}\csc\alpha$: 1 GHz	Nyquist rate of the signal
$m \geq 2N = 16$	$m \geq 2N = 16$	Number of sampling channels
$f_p = \frac{f_{NYQ}}{M} \geq B$	$u_p = \frac{u_{NYQ}}{M} \geq B_\alpha$	Frequency of each $p_i(t)$
$f_s \geq f_p = 10.53$ MHz	$u_s\csc\alpha \geq u_p\csc\alpha = 2.5$ MHz	Sampling frequency of a single channel
$L = 95 \leq \frac{f_{NYQ}}{B}$	$L = 400 \leq \frac{u_{NYQ}}{B_\alpha}$	Number of $p_i(t)$ changed times
$M_{min} = L = 95$	$M_{min} = L = 400$	Number of sign intervals in each $p_i(t)$
$mf_s \geq 160$ MHz	$mu_s\csc\alpha \geq 8$ MHz	The overall sampling rate for the system

$$\mathrm{NMSE} = \frac{\int_{-\infty}^{+\infty} |x(t) - \hat{x}(t)|^2 \mathrm{d}t}{\int_{-\infty}^{+\infty} |x(t)|^2 \mathrm{d}t}, \tag{34}$$

where $x(t)$ is the original signal. $\hat{x}(t)$ is denoted as the recovered signal.

We demonstrate the simulations for three different cases: robustness, recovery accuracy, and the influence of the order α. These comparisons show the recovery accuracy with different SNRs, the robustness when the signal is contaminated by Gaussian noise, and the influence of the fractional order α. Every simulation has 300 trials to ensure statistically stable results.

4.2. Robustness

We use expected restricted isometry property (ExRIP) to quantify the stability criterion.

Definition 1 (*ExRIP* [34]). A measurement matrix $\mathbf{\Psi}$ has the ExRIP, if RIP guarantees that $(1-\delta_k)\|x\|_2^2 \leq \|\mathbf{\Phi}z\|_2^2 \leq (1+\delta_k)\|z\|_2^2$ holds with a probability of at least p for K-sparse random vectors z, whose support is uniformly distributed and whose nonzeros are independent and identically distributed random variables.

The probability p is defined as follows:

$$p = 1 - \frac{M(1-C_K)(1+\boldsymbol{\alpha}(\mathbf{S}) - 2\boldsymbol{\beta}(\mathbf{S}))}{(M-1)\sigma_K^2} - \frac{M(B_K - C_K)(\boldsymbol{\gamma}(\mathbf{S}) - \boldsymbol{\beta}(\mathbf{S})) + M(M-1)C_K\boldsymbol{\beta}(\mathbf{S}) - 1}{(M-1)\sigma_K^2}, \tag{35}$$

where $\boldsymbol{\alpha}(\mathbf{S}) = \frac{1}{(mM)^2}\sum_{i,k=1}^{m}(\mathbf{S}_i^T\mathbf{S}_k)^2$ is defined as the correlation of the rows. $\boldsymbol{\beta}(\mathbf{S}) = \frac{1}{m^2M^3}\sum_{i,k=1}^{m}\|\mathbf{S}_i \odot \mathbf{S}_k\|^2$ is the total power of all auto-correlation and cross-correlation functions where the operator $\odot$ stands for cyclic convolution. $\boldsymbol{\gamma}(\mathbf{S}) = \frac{1}{(mM)^2}\sum_{i,k=1}^{m}(\mathbf{S}_i^T\mathbf{S}_k^-)^2$ where the vector $S_k[n] = S_k[-n]$, $n = 0, \ldots, M-1$ with module M. $C_K = \mathbb{E}\{\sum_{i=1}^{K}|z_i|^4/\|z\|^4\}$, and $B_K = \mathbb{E}\{|\sum_{i=1}^{K} z_i^2|^2/\|z\|^4\}$ are distribution-dependent constants. z_i are K random nonzero variables of z. B_K=1 whenever the nonzeros are real valued. $C_K = \frac{3}{2+K}$ when z_i are standard normal variables. It is easy to prove that the sensing matrix $\mathbf{S}$ has a high probability of satisfying the ExRIP.

The robustness of the system is evaluated by the probability of successful reconstruction in the noisy and noise-free cases. We compare the proposed system with the classic MWC system. Because the traditional Nyquist sampling can make full recovery, it is not necessary to compare the Nyquist sampling methods with the proposed method. The tradeoff between recovery probability and number of channels is evaluated in the noise-free case. Specifically, Fig. 8 depicts the performance when the number of active bands N is $\{4, 6, 8\}$. The number of channels varies from 4 to 60 with a step of 2. It is observed that the proposed system can use the limited number of channels to recover the signal, and more bands corresponding to more channels. It is clear that the original signal can be perfectly recovered when the number of channels is approximately 20, but the classic MWC cannot completely recovery the original signal. The overall sampling rate of MWC is $mf_s \approx 210$ MHz. The total sampling rate of the proposed method is $mu_s\csc\alpha \approx 50$ MHz. The probability of successful recovery dramatically increases when the number of channels becomes close to the theoretical value, which can be obtained by the ExRIP.

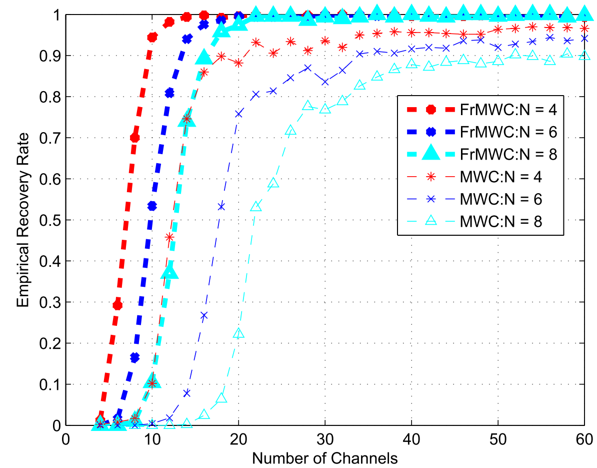

Fig. 8. Performance of recovery probability with different numbers of channels for noise-free signal.

In the noisy case, the simulations are demonstrated in two aspects, including the tradeoff between successful recovery probability and the number of channels and the balance between successful recovery rate and signal-to-noise ratio (SNR). Each comparison is evaluated with two different conditions. Fig. 9(a) and (b) depict the tradeoff of the number of channels and successful rate. In Fig. 9(a), and the SNR is fixed to 20 dB, and the number of bands is $\{4, 6, 8\}$. In Fig. 9(b), the SNR is $\{10, 15, 20\}$ dB, and the number of bands is fixed to 6. In both simulations, the number of channels varies from 4 to 60 with a step of 2. It is observed that the requirement of the number of channels depends on the number of bands, where more bands and a smaller SNR correspond to more channels. Occasionally, a low SNR may lead to failure of the recovery. Fig. 9(c) and (d) depict the tradeoff of SNR and successful rate. In Fig. 9(c), the number of bands is $\{4, 6, 8\}$, the number of channels is fixed to 20. In Fig. 9(d), the number of bands is fixed to 6, and the number of channels is $\{10, 15, 20\}$. The SNR varies from 1 dB to 35 dB with a step of 2 dB. It is observed that the probability of a successful recovery has the same trend aa the SNR. Although the chirp signal is bandlimited in the FD, the classic MWC cannot effectively reconstruct the signal. The proposed method shows better robustness than the classic MWC under various noise conditions and numbers of channels.

Fig. 10 depicts the performance in terms of successful rate with different SNRs and numbers of channels for the proposed method and the classic MWC. The number of bands is fixed to 6. The SNR varies from 5 dB to 35 dB with a step of 2 dB. The number of channels varies from 10 to 60 with a step of 2. The classic MWC is not suitable for fractional bandlimited signals because the successful recovery probability cannot reach one hundred percent even with more channels.

4.3. Recovery accuracy

The error between the original signal and recovered signal is mainly produced by the noise and potentially wrong indices in the recovered support. The recovery accuracy of the system is evaluated with different noise conditions. We compare the proposed system with the classic

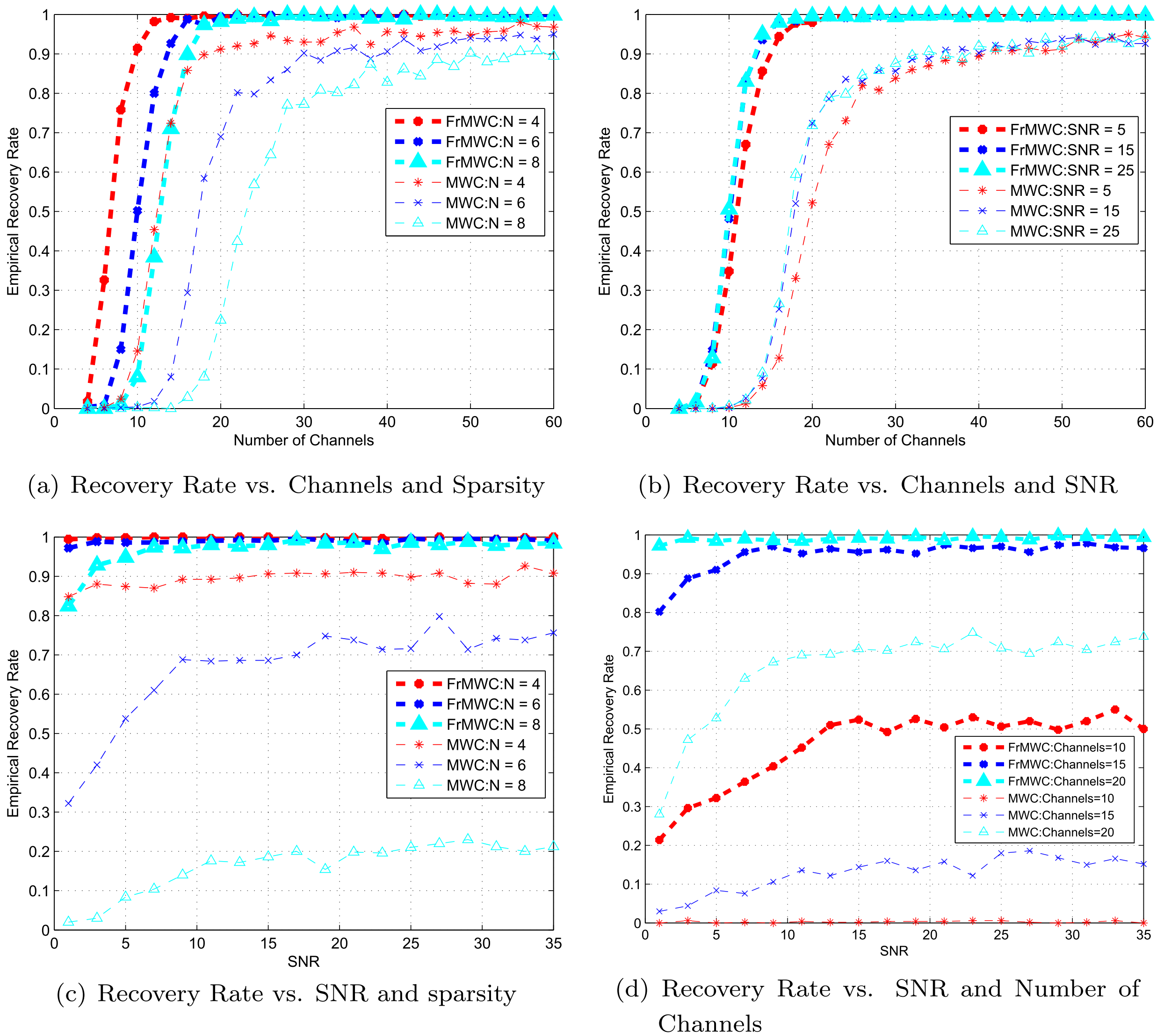

(a) Recovery Rate vs. Channels and Sparsity

(b) Recovery Rate vs. Channels and SNR

(c) Recovery Rate vs. SNR and sparsity

(d) Recovery Rate vs. SNR and Number of Channels

Fig. 9. Performance of robustness for the noisy signal.

MWC. Fig. 11 has the same conditions as Fig. 9 for every subfigure. Fig. 11 shows the relationship between the NMSE and SNR. It is common that the NMSE decreases with increasing SNR and the number of channels in both the proposed method and classic MWC. Fig. 11(a) and (b) show that increasing the channels leads to a decrease of the NMSE. The NMSE almost decreases to zero in the proposed

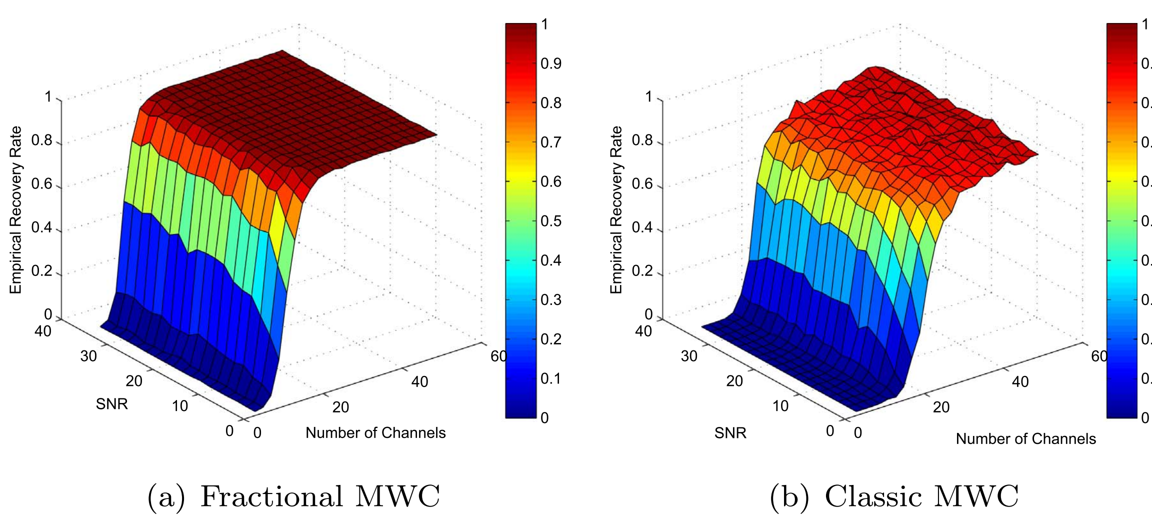

(a) Fractional MWC

(b) Classic MWC

Fig. 10. Performance of recovery probability in 3D space.

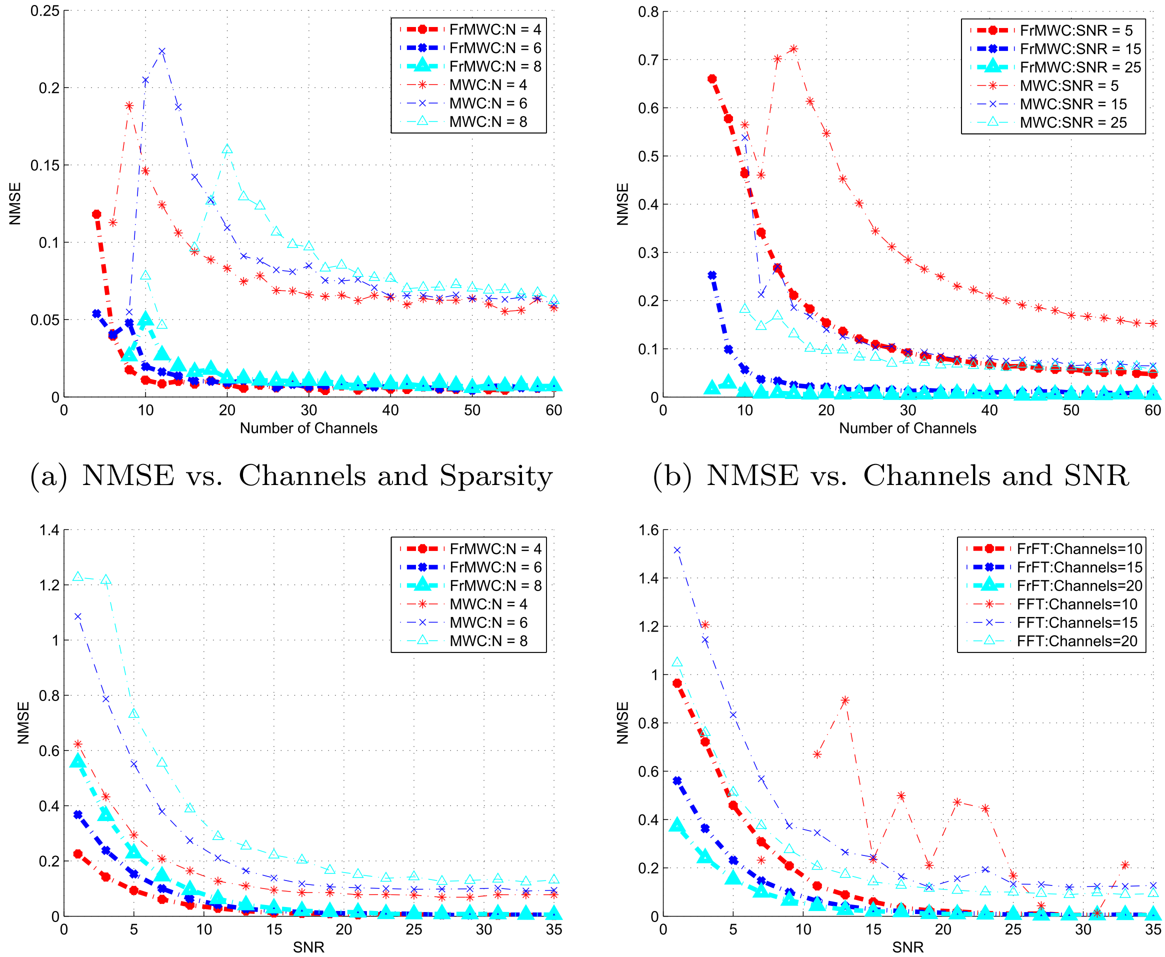

(a) NMSE vs. Channels and Sparsity

(b) NMSE vs. Channels and SNR

(c) NMSE vs. SNR and Channels

(d) NMSE vs. SNR and Channels

Fig. 11. Performance of recovery accuracy for noisy signal.

system, but the remaining NMSE in the classic MWC cannot reach zero. The performance of the tradeoff between the SNR and successful rate is shown in Fig. 11(c) and (d). MWC is intolerable for noise. It is clear that the proposed method has better recovery accuracy.

Fig. 12(a) and (b) show the performance in terms of reconstructed accuracy of the proposed method and MWC respectively. Fig. 12 has the same parameters as Fig. 10. The results marked in red are zeros because the recovery probability is zero. The largest NMSE of the

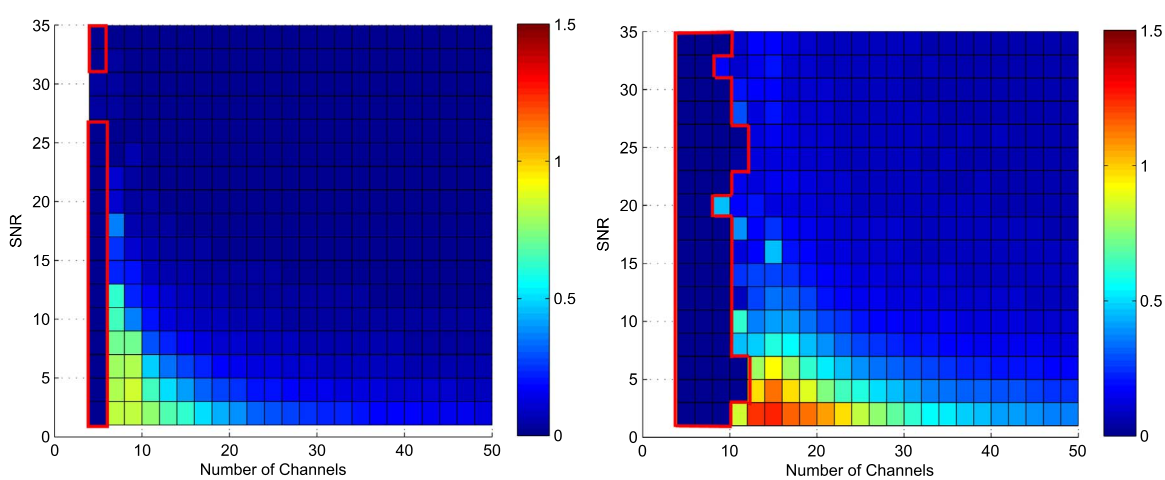

(a) Fractional MWC

(b) Classic MWC

Fig. 12. Performance of NMSE in the 3D space.

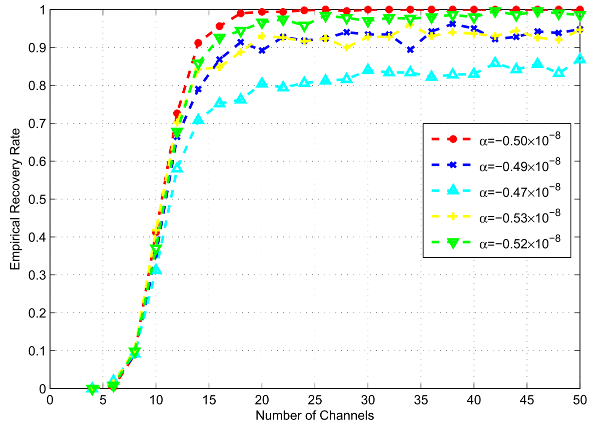

Fig. 13. Simulation of influence of the fractional orders.

proposed method is 0.85, which is generated based on the small successful recovery probability, and the largest NMSE of MWC is 1.45. The NMSE of the proposed method rapidly decreases when the number of channels reaches the theoretical value, and the classic MWC exhibits worse accuracy overall.

4.4. Simulation of influence of the order α

The prior fractional order α is an important factor that decides the bandwidth of the signals. Consequently, it partially influences the successful recovery probability. According to the foregoing analysis, an inaccurate order α may lead to changes in the spectral width. If the bandwidth of the real spectrum is wider than the bandwidth of the theoretical order, then the real maximum bandwidth will be bigger than the sampling rate. This will result in spectrum aliasing. The successful recovery rate will rapidly decrease. Fig. 13 shows the results of successful recovery with different fractional orders. The signal is the same as above. The number of bands is 6. The SNR is 15 dB. The orders are chosen to be $\{-0.50, -0.52, -0.53, -0.49, -0.47\} \times 10^{-8}$. The system has better tolerance for the error of fractional order when the sampling rate is larger than the maximum bandwidth of the signal. The result for the order -0.52×10^{-8} is almost the same as that with -0.50×10^{-8}. The bandwidth in -0.47×10^{-8} may exceed the previously proposed bandwidth.

5. Conclusion

This paper introduces a multichannel compressed sampling method for the multiband signals in the FrFD. The theory combines the modulated wideband converter with a sampling method in the FrFD that is easy to implement with the mixing and convolution in the time domain. The proposed system does not suffer from the high sampling rate issue. The simulation shows that the method is feasible and robust against additive Gaussian noise. Our results can be extended to the linear canonical transform domain. There is also future work to perform before the system can be placed into practice, including investigations into the transform angle or the bandlimited angle α.

References

[1] V. Namias, The fractional order Fourier transform and its application to quantum mechanics, IMA J. Appl. Math. 25 (3) (1980) 241–265.
[2] L.B. Almeida, The fractional Fourier transform and time-frequency representations, IEEE Trans. Signal Process. 42 (11) (1994) 3084–3091.
[3] H.M. Ozaktas, O. Arikan, M.A. Kutay, G. Bozdagi, Digital computation of the fractional Fourier transform, IEEE Trans. Signal Process. 44 (9) (1996) 2141–2150.
[4] S.-C. Pei, M.-H. Yeh, C.-C. Tseng, Discrete fractional Fourier transform based on orthogonal projections, IEEE Trans. Signal Process. 47 (5) (1999) 1335–1348.
[5] S.-C. Pei, J.-J. Ding, Closed-form discrete fractional and affine Fourier transforms, IEEE Trans. Signal Process. 48 (5) (2000) 1338–1353.
[6] M.A. Kutay, H.M. Ozaktas, O. Ankan, L. Onural, Optimal filtering in fractional Fourier domains, IEEE Trans. Signal Process. 45 (5) (1997) 1129–1143.
[7] M. Martone, A multicarrier system based on the fractional Fourier transform for time-frequency-selective channels, IEEE Trans. Commun. 49 (6) (2001) 1011–1020.
[8] L. Qi, R. Tao, S. Zhou, Y. Wang, Detection and parameter estimation of multicomponent LFM signal based on the fractional Fourier transform, Sci. China Ser. F: Inf. Sci. 47 (2) (2004) 184–198.
[9] R. Tao, B. Deng, W.-Q. Zhang, Y. Wang, Sampling and sampling rate conversion of band limited signals in the fractional Fourier transform domain, IEEE Trans. Signal Process. 56 (1) (2008) 158–171.
[10] E. Sejdić, I. Djurović, L. Stanković, Fractional Fourier transform as a signal processing tool: an overview of recent developments, Signal Process. 91 (6) (2011) 1351–1369.
[11] X.-G. Xia, On bandlimited signals with fractional Fourier transform, Signal Process. Lett., IEEE 3 (3) (1996) 72–74.
[12] F. Zhang, R. Tao, Y. Wang, Multi-channel sampling theorems for band-limited signals with fractional Fourier transform, Sci. China Ser. E: Technol. Sci. 51 (6) (2008) 790–802.
[13] J. Shi, Y. Chi, N. Zhang, Multichannel sampling and reconstruction of bandlimited signals in fractional Fourier domain, Signal Process. Lett. IEEE 17 (11) (2010) 909–912.
[14] L. Xu, F. Zhang, R. Tao, Randomized nonuniform sampling and reconstruction in fractional Fourier domain, Signal Process. 120 (2016) 311–322.
[15] A. Bhandari, A.I. Zayed, Shift-invariant and sampling spaces associated with the fractional Fourier transform domain, IEEE Trans. Signal Process. 60 (4) (2012) 1627–1637.
[16] X. Liu, J. Shi, X. Sha, N. Zhang, A general framework for sampling and reconstruction in function spaces associated with fractional Fourier transform, Signal Process. 107 (2015) 319–326.
[17] D.L. Donoho, Compressed sensing, IEEE Trans. Inf. Theory 52 (4) (2006) 1289–1306.
[18] J.N. Laska, S. Kirolos, M.F. Duarte, T.S. Ragheb, R.G. Baraniuk, Y. Massoud, Theory and implementation of an analog-to-information converter using random demodulation, in: Proceesings of IEEE International Symposium on Circuits and Systems (ISCAS 2007), IEEE, 2007, pp. 1959–1962.
[19] J. Lei, W. Liu, S. Liu, Q. Liu, Multiscale reconstruction algorithm for compressed sensing, ISA Trans. 53 (4) (2014) 1152–1167.
[20] J. Tropp, J.N. Laska, M.F. Duarte, J.K. Romberg, R.G. Baraniuk, et al., Beyond Nyquist: efficient sampling of sparse bandlimited signals, IEEE Trans. Inf. Theory 56 (1) (2010) 520–544.
[21] M. Mishali, Y.C. Eldar, From theory to practice: sub-Nyquist sampling of sparse wideband analog signals, IEEE J. Sel. Top. Signal Process. 4 (2) (2010) 375–391.
[22] M. Mishali, Y.C. Eldar, O. Dounaevsky, E. Shoshan, Xampling: analog to digital at sub-Nyquist rates, IET, Circuits, Devices Syst. 5 (1) (2011) 8–20.
[23] G. Frigo, C. Narduzzi, Characterization of a compressive sensing preprocessor for vector signal analysis, IEEE Trans. Instrum. Meas. 65 (6) (2016) 1319–1330.
[24] H. Zhao, L. Qiao, Y. Chen, Modulated wideband convertor for α-bandlimited signals in fractional Fourier domain, in: Proceedings of 2016 17th International Carpathian Control Conference (ICCC), 2016, pp. 831–835. http://dx.doi.org/10.1109/CarpathianCC.2016.7501211
[25] Ç. Candan, H.M. Ozaktas, Sampling and series expansion theorems for fractional Fourier and other transforms, Signal Process. 83 (11) (2003) 2455–2457.
[26] T. Erseghe, P. Kraniauskas, G. Cariolaro, Unified fractional Fourier transform and sampling theorem, IEEE Trans. Signal Process. 47 (12) (1999) 3419–3423.
[27] A.I. Zayed, On the relationship between the Fourier and fractional Fourier transforms, IEEE Signal Process. Lett. 3 (12) (1996) 310–311. http://dx.doi.org/10.1109/97.544785.
[28] P. Kraniauskas, G. Cariolaro, T. Erseghe, Method for defining a class of fractional operations, IEEE Trans. Signal Process. 46 (10) (1998) 2804–2807.
[29] A.I. Zayed, A.G. García, New sampling formulae for the fractional Fourier transform, Signal Process. 77 (1) (1999) 111–114.
[30] R. Baraniuk, M. Davenport, R. DeVore, M. Wakin, A simple proof of the restricted isometry property for random matrices, Constr. Approx. 28 (3) (2008) 253–263.
[31] H. Landau, Necessary density conditions for sampling and interpolation of certain entire functions, Acta Math. 117 (1) (1967) 37–52.
[32] M. Mishali, Y.C. Eldar, Reduce and boost: recovering arbitrary sets of jointly sparse vectors, IEEE Trans. Signal Process. 56 (10) (2008) 4692–4702.
[33] J.A. Tropp, A.C. Gilbert, M.J. Strauss, Algorithms for simultaneous sparse approximation. Part I: greedy pursuit, Signal Process. 86 (3) (2006) 572–588.
[34] M. Mishali, Y.C. Eldar, Expected RIP: conditioning of the modulated wideband converter, in: Proceedings of Information Theory Workshop, 2009 (ITW 2009), IEEE, 2009, pp. 343–347.